Molecular Oncologic Imaging 2025;5(1):01-16 *ISSN: 2791-965X*

Use of SPECT/CT in Scintigraphic Imaging Methods

Serap Nişli[1] Esra Arslan[2*] Mustafa Demir[3]

**Corresponding Author*

[1,2] Istanbul Training and Research Hospital, University of Health and Science, Clinic of Nuclear Medicine, Istanbul,Turkey

[3] Istanbul University Cerrahpaşa Faculty of Medicine, Department of Nuclear Medicine, Istanbul, Turkey

https://doi.org/10.71286/moi.1661510

Abstract

This study aims to acquire images of a human body phantom in two separate gantries (SPECT and CT), perform fusion of these images in a computer environment, determine the necessary criteria for this process, and analyze the clinical validity of the fusion process.

To quantify potential fusion errors in imaging for patients with movement restrictions, a unique phantom imaging setup was planned for this study. The data from the six different CT images and the single SPECT image taken at 0 degrees were uploaded to the DICOM system within the PMOD software program. The fusion process was then performed. It was observed that the fusion images exhibited deviations depending on the orientation angles, and these deviations increased proportionally with the angle.

The post-processing fusion of SPECT and CT images from separate gantries using a computer-based fusion program has some disadvantages. Patients must move to another department for CT imaging after undergoing SPECT, which can result in misalignment due to body movement. To correct these errors, the use of external markers becomes necessary. Another disadvantage is radiation safety concerns during patient transfers between imaging units due to the presence of radioactive material in the patient's body.

***Keywords*:** *SPECT CT, imaging, scintigraphy.*

INTRODUCTION AND OBJECTIVE

The purpose of medical imaging methods is to display the anatomical or functional condition of the entire human body or a specific region. The aim is to highlight details of the relevant region or to reveal lesions with sufficient detail in these images. In order to visualize lesions, their dimensions in spatial space must be within the resolution limits of the imaging system. Several factors can limit lesion detection, including:

- The contrast of the lesion relative to its surrounding tissue,
- The lesion's size and structure,
- The number of detected photons,

Address for Correspondence: Serap Nişli, Istanbul Training and Research Hospital, University of Health and Science, Clinic of Nuclear Medicine,Istanbul,Turkey **Phone:** +90 532 646 50 73 **E-mail:** serapnisli@hotmail.com **ORCID ID:** https://orcid.org/0009-0002-9463-8867

Received: 19.03.2025 Accepted: 05.05.2025 Published: .05.2025

- The lesion's depth and the extent of photon scattering and attenuation,
- The distance of the detector from the lesion,
- The angle at which the lesion is captured, potentially obscuring it entirely.

While planar imaging has several limitations, tomographic imaging has resolved many of these issues. Single-Photon Emission Computed Tomography (SPECT) combines functional imaging with anatomical imaging from Computed Tomography (CT), providing improved localization and more accurate scintigraphic findings.

This study aims to establish criteria for the fusion of CT and SPECT images taken from two separate gantries of a human body phantom. After completing the fusion process on the phantom, the study also aims to evaluate the clinical compatibility and validity of the determined criteria.

SPECT/CT is a hybrid imaging technology that integrates functional and anatomical patient data into a single image. It is among the latest advancements in modern imaging technology, where SPECT and CT systems are combined in a single unit. In SPECT imaging, anatomical differentiation of an organ that cannot be distinguished through scintigraphy alone is more easily and accurately achieved using fusion images (1).

CT plays critical roles in SPECT imaging. Accurate localization of anatomical structures and tumors that cannot be clearly identified in SPECT images and attenuation correction (2). When performing SPECT scans, the detector captures projection images from different angles around the organ of interest, but the number of detected photons varies with each projection. This occurs because photons travel through tissues of varying densities, experiencing different degrees of attenuation. CT images allow for the normalization of tissue densities, enabling attenuation correction.

- Lung density: 0.0296 g/cm²
- Soft tissue density: 0.0330 g/cm²
- Bone density: 0.0317 g/cm²

Even small differences in tissue density are accounted for in the imaging process. The grayscale values are obtained through daily quality control procedures using a Hounsfield phantom (3).

Various scintigraphic imaging techniques utilize SPECT as a routine method for lesion localization, although it has some limitations. By leveraging the existing resources in our clinic, we aim to fuse functional (SPECT) and morphological (CT) images to bridge the gap in anatomical imaging within nuclear medicine. This thesis was developed with the goal of contributing to the diagnostic accuracy of diseases by implementing SPECT/CT fusion imaging.

MATERIALS AND METHODS

Our prospective study was approved by the local ethics committee (2009/409), and all patients were asked for their verbal or written consent for the use of their individual clinical findings for research purposes.

SPECT Gamma Camera

SPECT images were acquired using a Mediso DHV Sprint dual-head variable-angle gamma camera equipped with a low-energy high-resolution parallel-hole collimator. The technical specifications of the gamma camera used in this study are detailed in Table 1.

Table 1: Technical Specifications of the Mediso DHV Sprint Gamma Camera

Parameter	Value
Useful Field of View (UFOV)	530 × 390 mm
Intrinsic Energy Resolution (UFOV, FWHM)	9.7%
Intrinsic Spatial Resolution (FWHM, CFOV)	3.6 mm
Intrinsic Spatial Resolution (FWHM, UFOV)	3.7 mm
Intrinsic Spatial Linearity (Differential, CFOV)	0.18 mm
System Spatial Resolution (LEAP/LEHR Collimator, FWHM)	8.9/7.3 mm

Anthropomorphic Human Body Phantom (Fillable Whole-Body Phantom)

To determine optimal imaging criteria for patients with movement restrictions, we utilized a custom-designed anthropomorphic phantom previously used for research in our department. This phantom was constructed to simulate a human body and allow for internal fluid filling to replicate background activity. The phantom was modeled after a 100 kg male patient with realistic dimensions. It was composed of three main sections: head and shoulders, lung and thoracic cage and pelvis and lower extremities.

For this study, only the lung-thoracic cage section was used. The lung compartment was designed as an elliptical chamber with a capacity of 30 liters of water, measuring 40 cm in height and 27–42 cm in diameter, constructed from 0.980 g/cm³ plexiglass material.

Phantom Lung Construction

The lung compartment was fabricated using a mold derived from a 100 kg human chest, ensuring realistic anatomical accuracy. The plexiglass sheet was thermoformed around a wooden mold in a high-temperature oven to match the curvature of the human ribcage. To allow for removable lung components, a 15 × 15 cm access port was integrated into the top of the phantom. The lungs were made from heated and molded 3 mm thick, 20 cm diameter plastic tubes, which were sealed at both ends with plexiglass plates. The lungs were filled with a 1:3 mixture of water (density: 1 g/cm³) and Styrofoam beads (density: 0.04 g/cm³) to match the approximate lung density of 0.35 g/cm³ (4). To replicate spinal vertebrae, a 4.5 cm diameter Teflon cylinder (density: 1.55 g/cm³) was placed inside the phantom. Rigid plastic ribs (density: 1.15 g/cm³) were also integrated into the lung-thoracic cage section.

Lesion Simulation in the Phantom

Lesions were designed to mimic small lung tumors (<3 cm in diameter) using plexiglass cylinders with densities of 0.980 g/cm³ and thicknesses of 1.5 mm. Four cylindrical lesions were created, with diameters of 0.6 cm, 1.0 cm, 1.6 cm, and 2.4 cm and a height of 2 cm. Each lesion had a 2 mm access hole sealed with a plug, allowing injection of water and radioactive material (Tc-99m).

The lesions were inserted into 10 cm long cylindrical tunnels within the lungs. To simulate realistic lesion densities, the interior of these cylindrical lesions was filled with a mixture of water and Styrofoam beads. Figure 1 depicts the phantom's lung-thoracic cage section, including the lesion placements.

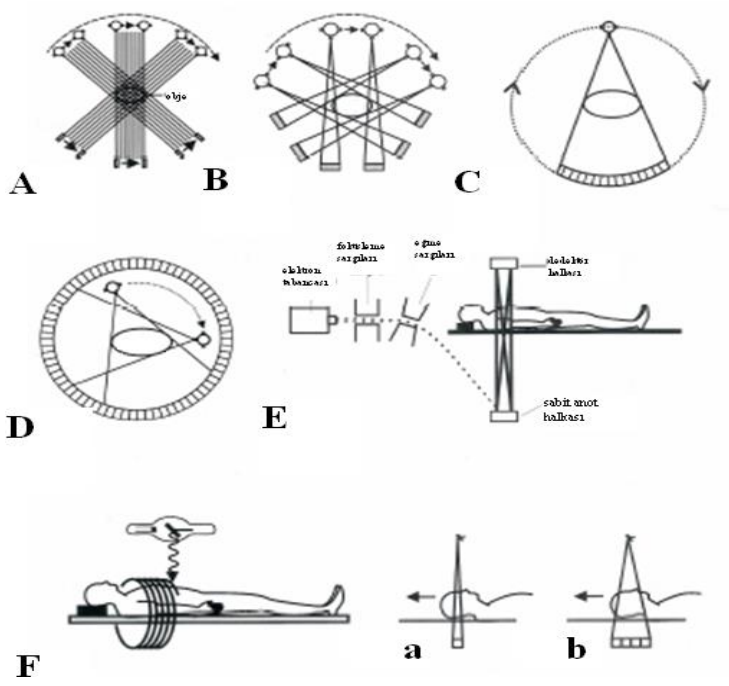

Figure 1: Evolution of CT Scanner Generations

- **A.** 1st Generation: Single detector and angled scanning
- **B.** 2nd Generation: Multiple detectors and angled scanning
- **C.** 3rd Generation: Tube and multiple detectors rotating together around the patient
- **D.** 4th Generation: Fixed detectors with a rotating tube
- **E.** 5th Generation: Electron beam CT developed for cardiac studies
- **F.** Helical (spiral) CT

    a) 6th Generation: Single-detector

b) 7th Generation: Multi-slice detector (18).

Selection of Markers for Fusion Imaging

Since SPECT and CT scans were performed on separate machines, a fusion software (PMOD) was used to manually align the images. To assist in this process, external reference markers were designed.

•**Material:** The markers were made of aluminum, which has low absorption in SPECT and minimal scattering in CT.

•**Design:** Cylindrical aluminum rods with a 1 cm outer diameter and a 0.5 cm hollow core were fabricated and cut into 1 cm segments.

•**Radioactivity Injection:** The hollow sections were filled with cotton, and a small amount of radioactive material (20–30 μCi of Tc-99m) was injected into the cotton.

•**Leak Prevention:** The markers were sealed with silicone tape to prevent leakage.

To ensure stable positioning, the radioactive markers were attached to the exterior of the phantom near the simulated lung lesions using medical adhesive tape.

Activity Levels Used in the Phantom

The activity concentration for lesions was determined by analyzing previous whole-body bone scintigraphy data from 25 patients. Ratio of background activity to lesion activity was calculated as 1:10 based on Region of Interest (ROI) analysis. To replicate realistic uptake values, the lung-thoracic cage section (30 liters) of the phantom was filled with 3 mCi (3000 μCi) of Tc-99m, yielding a background activity concentration of 1 μCi/ml. The lesions (8 ml total volume) were filled with 80 μCi of Tc-99m, resulting in a lesion activity concentration of 10 μCi/ml. This 1:10 lesion-to-background activity ratio was maintained across all imaging studies.

CT Imaging of the Phantom

To simulate real-world patient conditions, imaging began with CT scans before SPECT acquisition. The phantom was positioned on a PET/CT table, and external markers were affixed.

To analyze fusion errors in patients who require head support during scanning, the phantom was elevated at different angles (30°, 70°, 100°, 150°, and 200°) using foam support cushions under the head region. Figure 2 shows the different inclination angles used in the study.

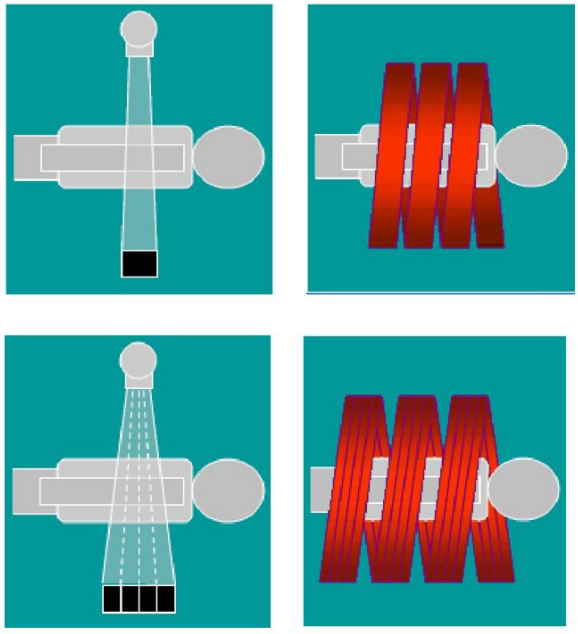

Figure 2: 6th and 7th Generation CT Systems

- Single-Slice System
- Single-Slice Helical System
- Multi-Slice System
- Multi-Slice Helical System
- Six separate CT scans were obtained at these angles.
- The torso section of the phantom was imaged in a transaxial orientation.
- These six CT images were used to evaluate orientation-induced fusion errors.

SPECT Imaging of the Phantom

SPECT imaging followed clinical protocols, using:

- 360° orbit
- 128×128×16 matrix
- 10-second projection time
- Parallel-hole LEHR collimator
- Bone filter for image processing

- Change attenuation correction method

The SPECT images were manually fused with CT images in the PMOD software, using the radioactive markers as alignment guides.

FUSION PROCESS AND CLINICAL EVALUATION

Analytical Fusion Program and Image Fusion Process

Advanced software analysis programs are used to further examine medical images. One such program is Pixel-Wise Kinetic Modeling (PMOD), which was employed in this study.

The PMOD software requires: A compatible operating system (Windows 2000, Linux, or MacOS), at least 1GB of memory, due to the program's high data storage requirements, Java runtime support for execution.

Key Features of PMOD Software

PMOD includes various image analysis tools and supports different configurations, allowing for a broad range of applications:

- DICOM compatibility enables loading of different medical image formats,
- Custom image layouts and color tables,
- Calculation of new slice images from existing data,
- Application of multiple image processing techniques,
- Display and registration of fusion images from different datasets,
- Correction of motion artifacts in dynamic imaging studies,
- Storage and export of fusion images as JPEG files,
- Direct identification of regions of interest (ROI) on fused images.

In PMOD, multi-modal fusion (PFUS) aligns images by using the first acquired dataset as the reference. Other datasets are adjusted to match its pixel size and slice thickness.

In our study, the CT and SPECT datasets of the phantom were loaded into PMOD's DICOM module. The datasets were then processed and aligned manually. The 0-degree CT scan (without inclination) served as the reference. Three anterior and lateral aluminum markers on the CT images were manually aligned with the corresponding radioactive markers in the SPECT images. No rotation adjustments were made, ensuring that only translational misalignments were corrected.

CLINICAL EVALUATION WITH SPECT/CT

To validate the fusion criteria established in the phantom study, we retrospectively analyzed patients who had undergone 111In-octreotide scintigraphy over the past year.

Patient Selection

Eight patients diagnosed with liver metastasis were selected. 4 men, 4 women, with an average age of 52.8±11.6 years (range: 33–67). 5 patients had carcinoid tumors, while 3 had neuroendocrine tumors (NETs) (Table 2).

Table 2: Patient Demographics

Patient No.	Age	Gender	Diagnosis
1	53	M	Carcinoid Tumor
2	41	F	Carcinoid Tumor
3	66	M	Carcinoid Tumor
4	58	M	Carcinoid Tumor
5	50	F	Carcinoid Tumor
6	55	F	NET
7	33	F	NET
8	67	M	NET

Imaging and Fusion Process

SPECT scans were performed using a Mediso DHV Sprint gamma camera. CT scans were obtained using a Siemens Biograph-6 PET/CT scanner (Figure 3 and 4). Fusion was conducted in PMOD software.

Two nuclear medicine specialists evaluated the planar, SPECT, and fused SPECT/CT images by analyzing only the liver region. Images were randomly analyzed without knowledge of patient identity. A segmental liver atlas was used to minimize localization errors.

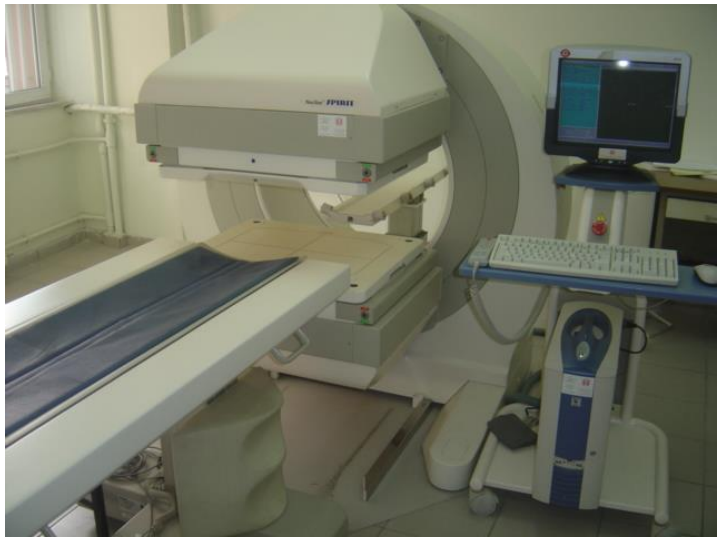

Figure 3: LEHR collimators were used with body contour attachment.

Figure 4: The CT scanner consists of a fast ceramic detector with the ability to acquire 6 slices.

Lesion Detection and Statistical Analysis

Reference fusion images were used as the gold standard. 126 lesions were detected in fusion images, 102 lesions were found in planar images, 120 lesions were identified in SPECT images.

Statistical Analysis

All data were analyzed with SPSS (Statistical Package for the Social Sciences) software for Windows (v19.0; IBM, Armonk, NY, USA). Individual and aggregate data were summarized using descriptive statistics, including mean, standard deviations, medians (min–max), frequency distributions, and percentages. Normality of data distribution was verified by Kolmogorov–Smirnov test. Comparison of the variables with normal distribution was made with the Students' t-test. Evaluation of categorical variables was performed by Chi-square test. The

kappa statistic was calculated to evaluate the agreement. p-Values of <0.05 were considered statistically significant.

SensitivityAnalysis

Compared to fusion imaging, the sensitivity of SPECT was 91.2%, while planar imaging had a sensitivity of 76.8%. Segmental analysis revealed differences in lesion detection across liver segments. SPECT was significantly more sensitive than planar imaging ($p<0.05$). Both SPECT and planar imaging had limited sensitivity for extrahepatic lesions (Table 3).

Table 3: Lesion Distribution by Liver Segment

Segment	Planar	SPECT	Fusion (Reference)
Segment 1	1	1	0
Segment 2	6	6	11
Segment 3	10	13	20
Segment 4	17	22	17
Segment 5	22	22	16
Segment 6	13	16	18
Segment 7	14	22	21
Segment 8	19	18	22
Total (Liver)	102	120	125
Extrahepatic Lesions	0	0	6

Key Findings

SPECT was significantly more sensitive than planar imaging ($p<0.05$) for total lesion detection. Planar imaging was notably weaker in identifying metastases in segment 3, 6, and 7. SPECT was particularly advantageous in segment 7 ($p<0.05$). Fusion imaging was superior in detecting extrahepatic metastases.

DISCUSSION

Hybrid imaging methods integrate anatomical information with functional data, significantly enhancing diagnostic accuracy. The most rapidly advancing hybrid imaging technique is PET/CT, but SPECT/CT has also proven valuable in localizing lesions by combining functional imaging with anatomical structure. This not only improves sensitivity but also enhances specificity in detecting abnormalities (6,7,8).

Several studies have shown that SPECT/CT improves image interpretation accuracy and clinical decision-making. It has been widely adopted in oncology, orthopedics, endocrinology, and infectious disease diagnostics (9-11). SPECT/CT is used in the preoperative localization of sentinel lymph nodes (SLNs) in cancers such as head and neck tumors, breast cancer, and cervical cancer. In a study, 43% of SLNs that were not visible on planar scintigraphy were detected using SPECT/CT (12). SPECT/CT has been particularly effective in overweight patients, where planar scintigraphy often fails (16). However, despite its advantages, SPECT/CT is not yet considered a standard procedure in breast cancer imaging. SPECT improves lesion localization, but its specificity is limited without anatomical correlation. SPECT/CT enhances lesion characterization, reducing the need for additional MRI or CT scans (17-19). In a retrospective study, 90% of indeterminate bone lesions on SPECT were accurately diagnosed with SPECT/CT (20). SPECT/CT enhances diagnostic accuracy in bone and soft tissue infections. It is particularly useful in orthopedic implant infections, differentiating between infection, trauma, and inflammation (24-31). Studies show that 3-phase bone scintigraphy combined with SPECT/CT has a 78% sensitivity and 86% specificity, compared to 50% specificity using SPECT alone (32). 131I scintigraphy is

highly sensitive for detecting thyroid cancer metastases, but it lacks anatomical reference markers. SPECT/CT reduces false positives caused by physiological iodine uptake (33,34). In parathyroid adenoma detection, SPECT/CT has been found superior to planar imaging, especially in ectopic adenomas or patients with altered neck anatomy (35-39). Somatostatin receptor imaging with 111In-octreotide is commonly used for neuroendocrine tumors. SPECT/CT improves lesion localization, leading to treatment modifications in up to 39% of cases (40,41). SPECT/CT is increasingly used in cardiac imaging, particularly in myocardial perfusion studies. CT attenuation correction significantly improves SPECT image quality and reduces artifacts from respiratory and cardiac motion (42-45). However, studies confirm that the diagnostic benefits outweigh these limitations, making SPECT/CT a valuable tool in nuclear medicine (46-50).

CONCLUSION

This study aimed to evaluate the feasibility of fusing SPECT and CT images acquired from separate gantries and assess its clinical accuracy. The small number of patients and the small number and variety of lesions are limitations of the study. However, the results obtained from studies that can be conducted with more cases and lesions will be beneficial to clinical practice. SPECT/CT should be preferred over planar or SPECT imaging alone in cases where precise anatomical localization is required. Fusion imaging improves diagnostic confidence, reducing false negatives and unnecessary additional scans. SPECT/CT should be considered in oncology, musculoskeletal imaging, infection diagnostics, and cardiac imaging. In conclusion, SPECT/CT represents a major advancement in nuclear medicine, providing both functional and anatomical insights in a single imaging session. Its clinical benefits are well established, and its use is expected to expand further in the future.

Peer-review: Externally peer-reviewed.

Authorship Contributions

Concept: S.N **Design:** S.N **Supervision:** E.A, S.N, M.D **Data Collection and/or Processing:** E.A, S.N, M.D **Analysis and/or Interpretation:** E.A, S.N, M.D **Literature Review:** E.A, S.N, M.D **Writer:** E.A, S.N

Conflict of Interest: No conflict of interest was declared by the authors.

Financial Disclosure: The authors declared that this study has received no financial support.

References

1. Römer W, Fiedler E, Pavel M et al. Attenuation correction of SPECT images based on separately performed. Nukleermedizin. 2005; 44: 20-8.
2. Preuss R, Weise R, Lindner O, Fricke H, Burchert W. Optimisation of protocol for low dose CT-derived attenuation correction in myocardial perfusion SPECT imaging. Eur J Nucl Mol Imaging. 2008; 35: 1133-41.
3. Goetze S, Brown TL, Lavely WC, Zhang Z, Bengel FM. Atteuation correction in myocardial SPECT/CT: effects of misregistration and value of reregistration. J Nucl Med. 2007; 48: 1090-5.
4. Coleman RE, Laymon CM, Turkington T. FDG imaging of lung Nodules: A phanton study comparing SPECT, camera-based PET, and dedicated PET. Radiology. 1999; 210: 823-8.
5. Mikolajczyk K, Szabatin M, Rudnicki P, Grodzki M, Burger C. A JAVA environment for medical image data analysis: initial application for brain PET quantitation. Med inform. 1998; 23: 207-14.
6. Czernin J, Allen-Auerbach M, Schelbert HR. Improvements in cancer staging with PET/CT: literature-based evidence as of September 2006. J Nucl Med. 2007; 48: 78-88.
7. von Schulthess GK, Steinert HC, Hany TF. Integrated PET/CT: current applications and future directions. Radiology. 2006; 238: 405-22.
8. Keidar Z, Israel O, Krausz Y. SPECT/CT in tumor imaging: technical aspects and clinical applications. Semin Nucl Med. 2003; 33: 205–18.
9. Even-Sapir E, Keidar Z, Sachs J et al. The new technology of combined transmission and emission tomography in evaluation of endocrine carcinomas. J Nucl Med. 2001; 42: 998–1004.
10. Pfanneberg AC, Eschmann SM, Horger M et al. Benefit of anatomical functional image fusion in the diagnostic work-up of neuroendocrine neoplasms. Eur J Nucl Med Mol Imaging. 2003; 30: 835–43.
11. Schillaci O. Functional–anatomical image fusion in neuroendocrine tumors. Cancer Biother Radiopharm. 2004; 19: 129–34.
12. Even-Sapir E, Lerman H, Lievshitz G, et al. Lymphoscintigraphy for sentinel node mapping using a hybrid SPECT/CT system. J Nucl Med. 2003; 44: 1413-20.
13. Sherif A, Garske U, de la Torre M, Thorn M. Hybrid SPECT-CT: an additional technique for sentinel node detection of patients with invasive bladder cancer. Eur Urol. 2006; 50: 83-91.
14. Khafif A, Schneebaum S, Fliss DM, et al. Lymphoscintigraphy for sentinel node mapping using a hybrid single photon emission CT (SPECT)/CT system in oral cavity squamous cell carcinoma. Head Neck. 2006; 28: 874-9.
15. Husarik DB, Steinert HC. Single-photon emission computed tomography/ computed tomography for sentinel node mapping in breast cancer. Semin Nucl Med. 2007; 37: 29-33.
16. Lerman H, Lievshitz G, Zak O, Metser U, Schneebaum S, Even-Sapir E. Improved sentinel node identification by SPECT/CT in overweight patients with breast cancer. J Nucl Med. 2007; 48: 201-6.
17. Hamaoka T, Madewell JE, Podoloff DA, Hortobagyi GN, Ueno NT. Bone imaging in metastatic breast cancer. J Clin Oncol. 2004; 22: 2942-53.
18. Minoves M. Bone and joint sports injuries: the role of bone scintigraphy. Nucl Med Commun. 2003; 24: 3-10.

19. Even-Sapir E. Imaging of malignant bone involvement by morphologic, scintigraphic, and hybrid modalities. J Nucl Med. 2005; 46: 1356-67.
20. Römer W, Nomayr A, Uder M, Bautz W, Kuwert T. SPECT-guided CT for evaluating foci of increased bone metabolism classified as indeterminate on SPECT in cancer patients. J Nucl Med. 2006; 47: 1102-6.
21. Horger M, Eschmann SM, Pfannenberg C, et al. Evaluation of combined transmission and emission tomography for classification of skeletal lesions. AJR. 2004; 183: 655-61.
22. Seo Y, Wong KH, Sun M, Franc BL, Hawkins RA, Hasegawa BH. Correction of photon attenuation and collimator response for a body-contouring SPECT/ CT imaging system. J Nucl Med. 2005; 46: 868-77.
23. Römer W, Reichel N, Vija HA, et al. Isotropic reconstruction of SPECT data using OSEM3D: correlation with CT. Acad Radiol. 2006; 13: 496-502.
24. Bar-Shalom R, Yefremov N, Guralnik L et al. SPECT/CT using 67Ga and 111In-labeled leukocyte scintigraphy for diagnosis of infection. J Nucl Med. 2006; 47: 587-94.
25. Kosuke Y, Noriaki M, Kazuki M, et al. Development of a new quantification method using partial volume effect correction for individual energy peaks in 111In-pentetreotide SPECT/CT. Asia Ocean J Nucl Med Biol. 2022 Spring;10(2):126-137.
26. Hope TA, Calais J, Zhang L, et al. 111In-pentetreotide scintigraphy versus 68Ga-DOTATATE PET: Impact on krenning scores and effect of tumor burden. J Nucl Med. 2019; 60(9):1266–9.
27. Finocchiaro D, Berenato S, Grassi E, et al. Partial volume effect of SPECT images in PRRT with 177Lu labelled somatostatin analogues: A practical solution. Phys Med. 2019; 57:153-9
28. Jönsson L, Stenvall A, Mattsson E, et al. Quantitative analysis of phantom studies of 111In and 68Ga imaging of neuroendocrine tumours. EJNMMI Phys. 2018; 20; 5(1):5.
29. Wickberg E, van Essen M, Rydén T, et al. EVALUATION OF THE SPATIAL RESOLUTION IN MONTE CARLO-BASED SPECT/CT RECONSTRUCTION OF 111IN-OCTREOTIDE IMAGES. Radiat Prot Dosimetry. 2021 Oct 12;195(3-4):319-326.
30. Mahsa Noori-Asl. Assessment of Four Scatter Correction Methods in In-111 SPECT Imaging: A Simulation Study. J Med Phys. 2020 Apr-Jun;45(2):107-115.
31. Ingui CJ, Shah NP, Oates ME. Infection scintigraphy: added value of singlephoton emission computed tomography/computed tomography fusion compared with traditional analysis. J Comput Assist Tomogr. 2007; 31: 375-80.
32. Horger M, Eschmann SM, Pfannenberg C, et al. Added value of SPECT/CT in patients suspected of having bone infection: preliminary results. Arch Orthop Trauma Surg. 2007; 127: 211-21.
33. Ingui CJ, Shah NP, Oates ME. Endocrine neoplasm scintigraphy: added value of fusing SPECT/CT images compared with traditional side-by-side analysis. Clin Nucl Med. 2006; 31: 665-72.
34. Tharp K, Israel O, Hausmann J, et al. Impact of 131I-SPECT/CT images obtained with an integrated system in the follow-up of patients with thyroid carcinoma. Eur J Nucl Med Mol Imaging. 2004; 31: 1435-42.
35. Yamamoto Y, Nishiyama Y, Monden T, Matsumura Y, Satoh K, Ohkawa M. Clinical usefulness of fusion of 131I SPECT and CT images in patients with differentiated thyroid carcinoma. J Nucl Med. 2003; 44: 1905-10.
36. Lavely WC, Goetze S, Friedman KP, et al. Comparison of SPECT/CT, SPECT, and planar imaging with single- and dual-phase 99mTc-sestamibi parathyroid scintigraphy. J Nucl Med. 2007; 48: 1084-9.
37. Harris L, Yoo J, Driedger A, et al. Accuracy of technetium-99m SPECT-CT hybrid images in predicting the precise intraoperative anatomical location of parathyroid adenomas. Head Neck. 2008; 30: 509-17.
38. Ruf J, Seehofer D, Denecke T, et al. Impact of image fusion and attenuation correction by SPECT-CT on the scintigraphic detection of parathyroid adenomas. Nuklearmedizin. 2007; 46: 15-21.
39. Krausz Y, Bettman L, Guralnik L, et al. Technetium-99m-MIBI SPECT/CT in primary hyperparathyroidism. World J Surg. 2006; 30:76–83.
40. Avram AM, Fig LM, Gross MD. Adrenal gland scintigraphy. Semin Nucl Med. 2006; 36: 212-27.
41. Even-Sapir E, Keidar Z, Sachs J, et al. The new technology of combined transmission and emission tomography in evaluation of endocrine neoplasms. J Nucl Med. 2001; 42: 998-1004.

42. Dondi M, Fagioli G, Salgarello M, Zoboli S, Nanni C, Cidda C. Myocardial SPECT: what do we gain from attenuation correction (and when)? Q J Nucl Med Mol Imaging. 2004; 48: 181-7.
43. Masood Y, Liu YH, Depuey G, et al. Clinical validation of SPECT attenuation correction using x-ray computed tomography-derived attenuation maps: multicenter clinical trial with angiographic correlation. J Nucl Cardiol. 2005; 12: 676-86.
44. Madsen MT. Recent advances in SPECT imaging. J Nucl Med. 2007; 48: 661-73.
45. Goetze S, Wahl RL. Prevalence of misregistration between SPECT and CT for attenuation-corrected myocardial perfusion SPECT. J Nucl Cardiol. 2007; 14: 200-6.
46. Krausz Y, Keidar Z, Kogan I, et al. SPECT/CT hybrid imaging with 111In-pentetreotide in assessment of neuroendocrine tumours. Clin Endocrinol. 2003; 59: 565-73.
47. Hillel PG, van Beek EJ, Taylor C, et al. The clinical impact of a combined gamma camera/CT imaging system on somatostatin receptor imaging of neuroendocrine tumours. Clin Radiol. 2006; 61: 579-87.
48. Kloppel G, Perren A, Heitz PU. The gastroenteropancreatic neuroendocrine cell system and its tumors: the WHO classification. Ann N Y Acad Sci. 2004; 1014: 13-27.
49. Veenhof CH, de Wit R, Taal BG et al. A dose-escalation study of recombinant interferon-alpha in patients with a metastatic carcinoid tumour. Eur J Cancer. 1992; 28: 75-8.
50. Solcia E, Klöppel G, Sobin LH, et al. Histological typing of endocrine tumours. 2nd Ed. WHO International Histological Classification of Tumours. Springer. Berlin. 2000.